Available online at www.sciencedirect.com

ScienceDirect

Energy Procedia 4 (2011) 4945–4952

Energy Procedia

www.elsevier.com/locate/procedia

GHGT-10

Exploring capillary trapping efficiency as a function of interfacial tension, viscosity, and flow rate

Dorthe Wildenschild[a]*, Ryan T. Armstrong[a], Anna L. Herring[a], Iain M. Young[b], and J. William Carey[c]

[a]*School of Chemical, Biological and Environmental Engineering, Oregon State University, Corvallis, OR, USA*
[b]*School of Environmental and Rural Sciences, University of New England, NSW, Australia*
[c]*Earth and Environmental Sciences Division (EES), Los Alamos National Laboratory, Los Alamos, NM, USA*

Abstract

We present experimental results based on computed x-ray microtomography (CMT) for quantifying capillary trapping mechanisms as a function of fluid properties using several pairs of analog fluids to span a range of potential supercritical CO_2-brine conditions. Our experiments are conducted in a core-flood apparatus using synthetic porous media and we investigate capillary trapping by measuring trapped non-wetting phase area as a function of varying interfacial tension, viscosity, and fluid flow rate. Experiments are repeated for a single sintered glass bead core using three different non-wetting phase fluids, and varying concentrations of surfactants, to explore and separate the effects of interfacial tension, viscosity, and fluid flow rate. Analysis of the data demonstrates distinct and consistent differences in the amount of *initial* (i.e. following CO_2 injection) and *residual* (i.e. following flood or WAG scheme) non-wetting phase occupancy as a function of fluid properties and flow rate. Further experimentation and analysis is needed, but these preliminary results indicate trends that can guide design of injection scenarios such that both initial and residual trapped gas occupancy is optimized.

Keywords: capllary trapping; residual phase; x-ray tomography; interfacial tension, viscosity, flow rate

1. Introduction

With large untapped coal reserves in the US and several other industrialized countries, it is highly likely that combustion of coal and coal-derived products will be part of the global energy future. Compared to other fossil fuels, coal-based power yields the highest CO_2 output per energy unit, indicating the need for some form of carbon mitigation [1] regardless of the predicted climate change scenario [2]. Geological sequestration of the captured CO_2 is the most mature in terms of large-scale deployment [2] and it is therefore an attractive and necessary carbon mitigation strategy. Geological carbon sequestration, however, also carries substantial risks such as leakage (acute or sustained) of the injected gas back into the vadose zone and atmosphere through abandoned wells or fracture and fault systems. Despite very broad research efforts by industry, government, and academic groups, there are still

* Corresponding author. Tel.: +1-541-737-8050; fax: +1-541-737-4600.
E-mail address: dorthe@engr.orst.edu.

doi:10.1016/j.egypro.2011.02.464

substantial uncertainties related to the effectiveness of the trapping, dissolution, and precipitation processes controlling the permanent storage of CO_2 [3].

Typical sequestration scenarios involve the injection of supercritical CO_2 into the aquifer while displacing brine in what is equivalent to a water drainage process. Due to density differences between supercritical CO_2 and reservoir brine, the CO_2 will buoyantly migrate upward until an impermeable barrier is encountered. Once injection stops, buoyant forces will continue to propel the CO_2 upwards, while brine reoccupies the pore space in a water imbibition process, trapping some of the CO_2. Depending on the dissolution kinetics of the host rock, the ultimate fate of the CO_2 is a carbonate mineral precipitate – a process that may take thousands of years to complete.

Four trapping mechanisms can be identified in this sequestration process: (1) *structural trapping,* in which CO_2 is trapped according to density and controlled by the geology of the storage zone, (2) *dissolution trapping,* which represents CO_2 dissolved in brine and/or oil (e.g.[4, 5]), (3) *mineral trapping,* where carbonate minerals are formed and, (4) *capillary trapping* sometimes referred to as residual trapping or relative permeability hysteresis trapping (e.g. [6-11]). In the capillary trapping process, CO_2 is immobilized by the imbibition process where capillary interactions lock isolated CO_2 bubbles in place at the pore-scale, thus preventing large-scale movement of CO_2 within the saline aquifer. Capillary trapping takes place when saline water imbibes back into the formation, *after* injection (i.e. water drainage) has stopped.

Capillary trapping has several advantages over structural trapping. Firstly, CO_2 is trapped by capillary forces that are greater than buoyant forces, meaning that rather than being constrained by potentially compromised reservoir caprock, the CO_2 is held in place in pore-scale bubbles. Secondly, because the bubbles have a large surface-to-volume ratio, enhanced dissolution of CO_2 into the brine is facilitated. Thirdly, the capillary trapping mechanism allows CO_2 to be distributed over a larger reservoir volume, thus allowing access to a larger rock volume for mineral weathering and carbonate deposition. Despite not necessarily increasing the volume of CO_2 that can be injected, these combined secondary effects significantly improve storage security [12]. Capillary trapping is therefore a crucial process with small-scale physical controls that must be understood in detail in order to sequester CO_2 at large spatiotemporal scales.

In recent work, [13, 14] measured trapped non-wetting phase saturation as a function of initial saturation in sand packs, and compared the resulting curves to various trapping model expressions. They concluded that the data was poorly matched by one of the more commonly used trapping models (Land's [15]) that relates trapped residual gas saturation to initial gas saturation, but found that a two-slope model [16] provided a better fit. Similar work was reported by [17]. [18] also recently conducted experimental work to directly address capillary trapping phenomena, and the work of [19] indirectly addresses capillary trapping, yet, there is still a great need for more experimentation.

The aim of the present work is to increase our understanding of the capillary trapping mechanism, in particular how fluid characteristics influence trapping efficiency, and whether injection scenarios can be designed to achieve optimal trapping capacity. This was addressed by measuring amounts of trapped non-wetting phase after injection (drainage) and also upon imbibition for a range of non-wetting phase fluid interfacial tensions (IFTs), viscosities, and also for different flow rates. Various non-wetting phase fluids (air, octane, and Soltrol 220) were used as proxies for CO_2 at sub or supercritical conditions, and the wetting phase was a brine solution providing good x-ray contrast. The trapped initial and residual non-wetting phase amounts were measured using high-resolution x-ray microtomography, and the relationship between initial and residual trapped areal occupancies was established for a preliminary assessment. To our knowledge, this is the first study of the effect of fluid characteristics such as interfacial tension and viscosity on the efficiency of non-wetting phase trapping.

2. Materials and methods

All experiments were conducted on a single sintered glass-bead core, 6.35 mm i.d. and 3.5 cm tall. The core was sintered at 675 ^{o}C. The soda-lime glass beads consisted of a mixture of three sizes: 35% 0.6 mm, 35% 0.8 mm, and 30% 1.0-1.4 mm diameter. The fluids used were a KI-brine (7.5% KI by weight) for the wetting fluid, and three different non-wetting fluids (all less dense than brine) as listed in Table 1. The fluid interfacial tensions, viscosites, and densities represent CO_2 under varying sub- and supercritical conditions for different pressures, temperatures, and salinities as reported by [2, 20, 21]. We refer to brine displacing non-wetting fluid as imbibition, and to non-wetting fluid displacing brine as drainage. The glass bead core was contained in an Aluminum (3003 alloy) core holder with a 0.3 mm wall thickness, and with a semi-permeable, hydrophilic membrane (Nylaflo Nylon Membrane, 0.2 mm) placed at the bottom of the column to prevent non-wetting phase from entering the brine line. The brine line was connected to a syringe pump, which precisely controlled the amount of brine pumped into and out of the

porous medium, see [22] for details. Non-wetting fluids entered through the top. The oils used contained Oil Red O and the interfacial tensions listed in Table 1 were measured with this dye.

Table 1. Fluid characteristics

	Non-wetting fluids						
	air	octane	Soltrol 220				
Interfacial tension w. KI-brine (dynes/cm)	72	37	17				
Viscosity (mPa-s = cP)	0.018	0.54	4.82				
Density (g/cm^3)	0.001	710	790				
	Wetting fluids						
	brine	Triton #1	Triton #2	Triton #3	Triton #4	Triton #5	Triton #6
Interfacial tension w. air (dynes/cm)	72	37	44	47	55	60	70
Viscosity (mPa-s = cP)	1.13	1.13	1.13	1.13	1.13	1.13	1.13
Density (g/cm^3)	1080	1080	1080	1080	1080	1080	1080

The brine consisted of a KI-solution at a 1:12 mass ratio of KI:H_2O, which improved the contrast between brine and the solid and non-wetting phases sufficiently for segmentation in the CT images. Brines containing various concentrations of Triton 100X surfactant were also used to lower the interfacial tension and separate the effects of interfacial tension and viscosity on trapping efficiency (assuming that the very small amounts of surfactants added did not alter the brine viscosity). All experiments were conducted at atmospheric pressure and controlled temperature of 21-22 ^{o}C. The same sintered glass bead core was used in all experiments, and between experiments was removed from the core holder, cleaned with acetone, ethanol, and DI water, and dried with compressed air before replaced in the core holder again for the next experiment. This ensures that the starting condition is identical for all runs. The core was then saturated slowly with brine at a rate of 1 ml/hr to achieve full saturation. After saturation, a preset brine volume of 343 ml was drained from the core using the syringe pump, and after scanning, a brine volume of 327 ml was subsequently used on imbibition for all experiments.

By using the exact same boundary conditions and fluid volumes for each run, it is possible to directly compare the resulting amount of trapped fluid as a function of fluid characteristics. The core was imaged dry before the first experiment, and also after full saturation for 13 of the runs to ensure that full saturation was achieved (and thus that the wettability of the core holder had not changed by exposure to the various non-wetting fluids, i.e, that the cleaning procedure worked). Once we observed that our procedure ensured full saturation, the core was no longer imaged at full saturation to save scans and thereby time. After each pumping episode the core was left to equilibrate for approximately 10 minutes to ensure fluid equilibration. Capillary pressure was measured with a differential pressure transducer to track the pressure equilibration process and to help determine when equilibrium was reached. Ultimately, if the scans were blurry, indicating movement of interfaces during the scan, the core was re-scanned after additional equilibration time. The imaging was performed using computed x-ray microtomography (CT), in the School of Environmental and Rural Sciences at University of New England, Armidale, NSW, Australia. The system was a GE/Phoenix v|tome|x s ultra high-resolution CT system with a maximum resolution of 4 micron and a maximum x-ray voltage of 240 kV. All images were captured using the 240 kV tube, using a voltage of 95 kV, a current of 80 mA, and an image exposure time of 800 ms. The cores were imaged using 1000 angles, the detector was 512x512 voxels and the resulting image voxel size was 14.9 micron.

Image Processing and Quantitative Data Analyses.

We used the local intensity minimum between the non-wetting phase and solid/brine phase for the threshold value. A cubic (283x283x420 voxels) portion of the central part of the cylinder was cropped out for further analysis to eliminate potential wall effects. Figure 1 shows a couple of example images of the trapped non-wetting phase surface for the different viscosity/IFT pairs resulting from drainage at 2 ml/hr and subsequent imbibition also at 2 ml/hr. Gray-scale CT images require further image analysis to accurately quantify porosity, phase distributions, and other fluid-fluid variables. The wetting-, non-wetting- and solid-phase volume fractions can be quantified via a segmentation routine (using IDL®) and using the commercial program Avizo™. Details regarding our segmentation algorithm and its validation are available in [23]. For the present analysis, we used the total non-wetting phase surface area per volume as a proxy for non-wetting phase saturation. The areas between CO_2 and brine are the main drivers behind the mass transfer process that controls dissolution of CO_2 in brine, and are therefore of significant relevance for assessment of dissolution trapping of CO_2. The data was first filtered with a 2x2x2 kernel Gaussian filter, and then non-wetting phase surface areas were calculated using the marching cubes surface generating algorithm in Avizo. This approach was used because the non-wetting phase can be reliably separated from the other

phases (wetting, solid porous medium, and core holder) in terms of intensity and can therefore be easily segmented using a simple histogram threshold.

3. Results

Drainage and imbibition experiments were carried out at 3 different flow rates: 2, 5, and 10 ml/hr. In the base drainage cases brine was drained at 2 ml/hr to separate effects of drainage rate and resulting fluid distribution on the imbibition process. As predicted by various trapping models (see [14, 17]), the residual trapped non-wetting phase saturation depends on the initial non-wetting phase saturation, and we therefore conducted experiments at different drainage rates to establish a range of initial non-wetting phase saturations. In subsequent imbibition runs, we then combined these various drainage rates with different imbibition rates (2, 5 and 10ml/hr). The following discussion is based on non-wetting interfacial areas per volume as described above.

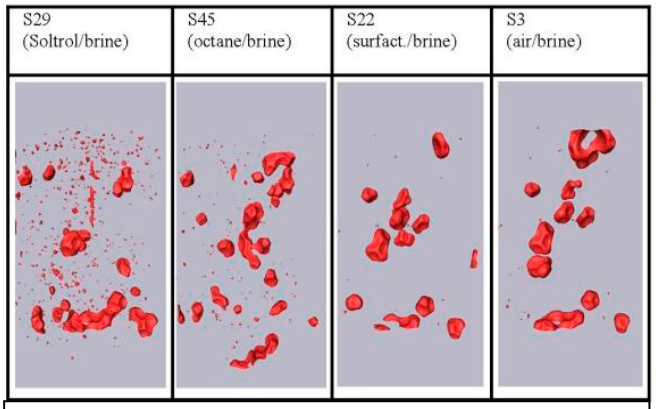

Figure 1. Non-wetting residual phase after 2 ml/hr drainage and 2 ml/hr imbibition **(S29)** Soltrol/brine (17 dynes/cm; 4.8 cP), **(S45)** octane/brine (37 dynes/cm; 0.54 cP), **(S22)** surfactant/brine (37 dynes/cm; 0.018 cP), **(S3)** air/brine (72 dynes/cm; 0.018 cP).

Effect of interfacial tension and viscosity

Figure 2 shows initial and residual non-wetting (NW) phase occupancy as a function of interfacial tension (IFT) for the various flow rates used. Despite some scatter in the data, there is a recognizable trend in *initial* non-wetting phase area with IFT (left-hand figure); the highest amount of initial NW phase saturation (i.e., the least efficient wetting fluid drainage) is obtained for the highest IFT, and for the lowest flow rate. Distinct trends are also seen for the various flow rates used, indicating that they play a role as well. For *residual* trapped NW phase areas (right-hand figure), we observed a distinct increasing trend with decreasing IFT. A decrease in IFT is expected to affect the NW phase blob morphology towards smaller and more numerous blobs, e.g. [24] and thus larger surface-to-volume ratios, yet, the example images in Figure 1 do not support that concept since the octane/brine and surfactant/brine at 37 dynes/cm look fairly similar, and if anything shows larger surface-to-volume ratio for the octane, thus indicating a trend with increasing viscosity instead. However, it needs to be emphasized that the viscosities of the fluids used in this study vary more than two orders of magnitude, while the IFTs vary only by a factor of ~4.

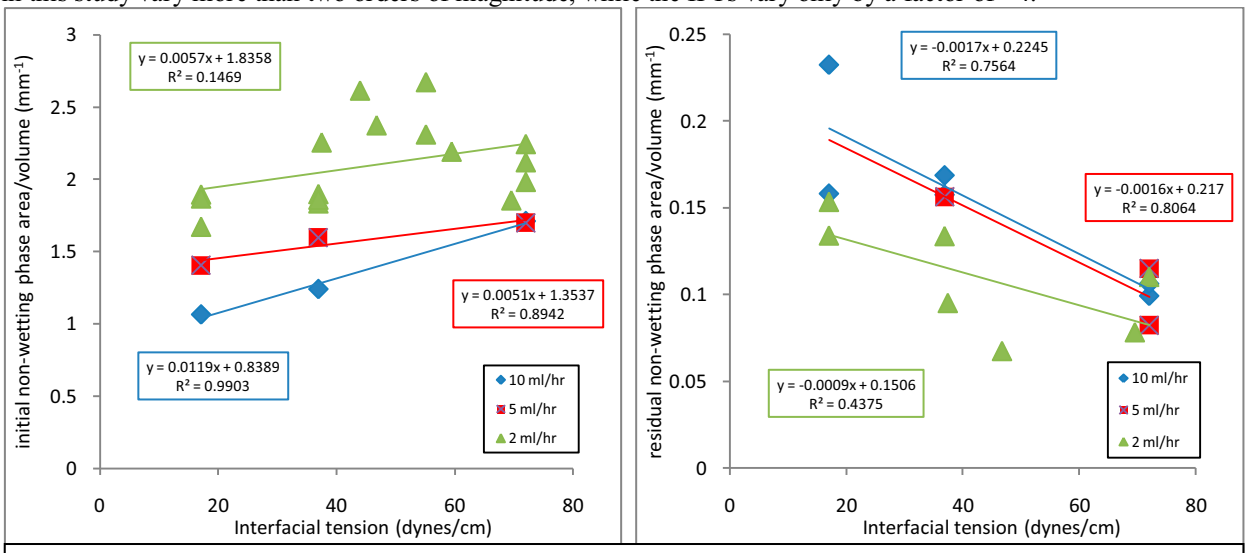

Figure 2. Initial (left) and residual (right) non-wetting phase area per volume as a function of fluid-fluid interfacial tension for three fluid flow rates.

The trend for *residual* trapping vs IFT (Figure 2 right) is also linear for each of the flow rates used. In both plots in Figure 2, the surfactant data (IFTs between ~40-70 dynes/cm, 2 ml/hr flow rate) is somewhat scattered, but

still adheres decently to a linear approximation. The linear trend lines in both plots also illustrate the increasing effect of flow rate with decreasing IFT (and/or viscosity), as the lines approach each other at the air and surfactant end of the IFT spectrum (see Figure 4 and discussion under flow rates). As a rule of thumb, it appears that trapped *initial* amount more than doubles with the chosen IFT and flow rate, whereas trapped residual amount almost triples.

Figure 3 shows NW phase areas as a function of NW phase viscosity, and clear trends are obvious for both *initial* and *residual* NW phase for this variable as well. For the *initial* NW phase area we see a linear decrease with increasing viscosity for each flow rate used, and the opposite is the case for the *residual* NW phase where we observe a very distinct linear increase in trapped NW phase area with increasing viscosity of the receding (NW) fluid, as well as fluid flow rate. As for IFT, the trend with flow rate diminishes for the lower viscosity (higher IFT) fluids.

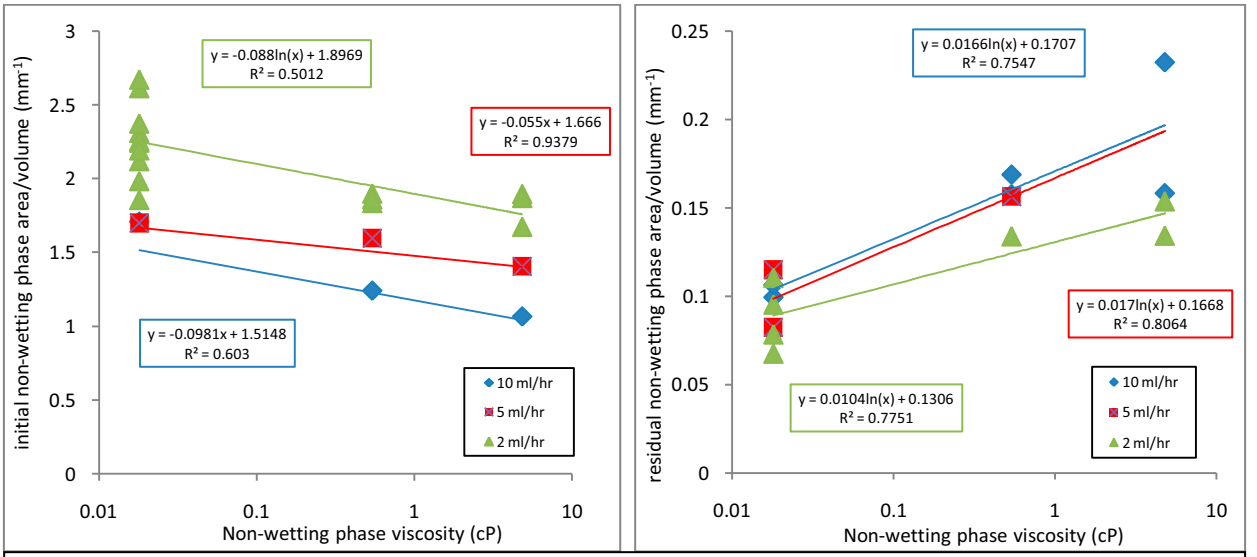

Figure 3. Initial (left) and residual (right) non-wetting phase area per volume as a function of non-wetting phase viscosity for three fluid flow rates.

Flow rate effects

In general, textbooks [25, 26], as well as experimental results, e.g. [27-30] predict that the necessary prerequisite for decreasing the amount of residual NW phase is an increase in capillary number (Ca), i.e., an increase in the ratio between viscous and capillary forces.

[31] explains this dependence of trapping on capillary number from the perspective of whether flow is dominated by frontal displacement or by snap-off, the latter resulting in larger amounts of trapped non-wetting phase. For a porous medium structure that otherwise facilitates snap-off (small contact angles, high aspect ratios), snap-off is favoured by low flow rates, whereas high flow rates suppress snap-off, and thus result in low trapped saturations.

Using one of the more common expressions for capillary number: $Ca = \frac{\mu_w v_w}{\sigma}$ where μ_w is the viscosity of the wetting fluid, v_w is the Darcy velocity of the wetting fluid, and σ is the interfacial tension between the wetting and non-wetting fluid, we see that a decrease in Ca can be achieved either by decreasing the viscosity or increasing the interfacial tension. It should be noted here that more than a dozen expressions have been used in the literature to express the ratio of viscous to capillary forces also known as capillary number [27]. In our imbibition experiments, the invading fluid (brine) is the same for all experiments, while the receding fluid varies, and therefore the NW fluid viscosity varies. If using the most commonly used expression for Ca, we will therefore only see a weak variation in Ca number among the different experiments, yet we believe the viscosity of the NW fluid is of importance as well. However, by examining Ca number, we lump together all three effects investigated here, and we have therefore chosen to present our data in terms of flow rate, IFT and viscosity. It should be noted though, that if we calculate Ca number based on non-wetting phase viscosity, we end up with values between 10^{-8} and 10^{-6}, and we observe a distinct decrease in trapped *initial* NW phase area with increasing Ca number, and likewise a clear increase in trapped *residual* NW phase with increasing Ca number.

To return to how we can decrease capillary number to facilitate more residual NW phase trapping, our results do not agree with the idea of either decreasing the viscosity (Figure 3, right) or increasing the IFT (Figure 2, right).

To examine the dependence of *initial* and *residual* phase occupancy on flow rate (separated from viscosity and IFT effects) Figure 4 shows both variables as a function of drainage and imbibition flow rate for the different fluid pairs. As discussed previously (Figure 2 and 3), a clear trend can be seen in Figure 4 for the amount of *initial* non-wetting phase (left figure) as a function of non-wetting fluid IFT and/or viscosity.

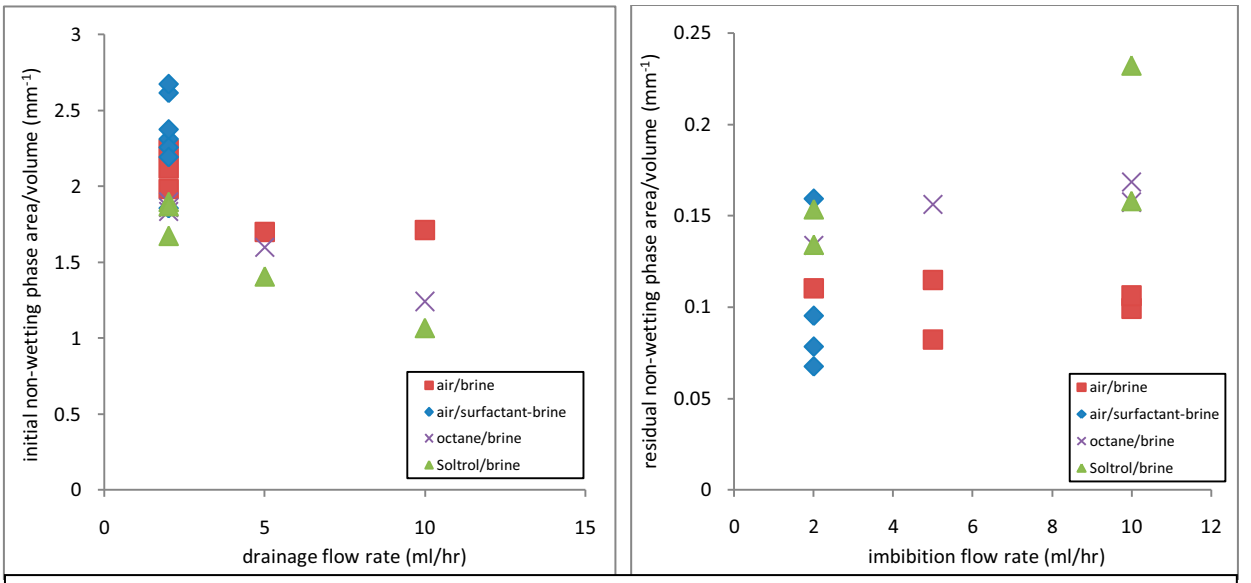

Figure 4. *Initial* (left) and *residual* (right) non-wetting phase area per volume as a function of brine drainage (left) and imbibition (right) flow rate for the various fluid pairs.

At 2 ml/hr the highest non-wetting phase occupation is obtained for the highest IFT and lowest viscosity, namely for the surfactant solutions. Decreasing amount of non-wetting phase is seen with decreasing IFT and increasing viscosity. A similar, or even stronger, trend with fluid IFT/viscosity is observed for the higher flow rates. In addition, increasingly less efficient drainage (more brine left, less non-wetting phase) is achieved with increasing flow rate for the higher viscosity fluids (octane and Soltrol). This result corresponds with the findings of [32] who also reported, based on x-ray CT studies, that increasing drainage flow rates resulted in less efficient drainage for an air-water-sand pack system. Despite the scatter within fluid pair data, a weak trend is also observed in the *residual* trapped amount with fluid IFT/viscosity, Figure 4 (right): we generally obtain increasing amounts of trapped non-wetting phase as the non-wetting fluid viscosity increases from 0.018 cP (air) to 0.54 cP (octane) to 4.8 cP (Soltrol). Interfacial tension appears less effective as both the air/brine and air/surfactant solutions (which cover IFTs between 37-72 dynes/cm) generally produce lower trapped amounts, see also example images in Figure 1. Because of the noise in the data, and limited number of data points, we are hesitant to suggest a definite trend in trapped amount with flow rate. The octane/brine and Soltrol data show a slight increase in trapped amount with flow rate, but the effect of flow rate is more clearly seen in Figure 2 (right) and 3 (right), where an increase in trapped *residual* amount with increasing flow rate is rather clearly defined. A trend of decreasing trapped residual with capillary number has been observed in many experiments e.g. by [11, 28-30, 33], but it should be kept in mind that most of these studies reported that there is a fairly distinct cut off at a Ca of approximately 10^{-6} below which trapped non-wetting phase is not affected by flow rate (or Ca). Our results suggest that a weak opposite trend may be present at low Ca, yet fairly distinct trends are observed for IFT and viscosity that also go against the previously reported rule of decreasing trapped gas amount with Ca number (since decreasing viscosity and increasing IFT also represent decreasing Ca). However, we emphasize that our coarse, unconsolidated system (and relatively low Ca) differs quite drastically from most of the porous media examined previously (tight rock cores), and additional experimentation and further analysis is needed to reliably establish trends. In similar studies on 600 micrometer diameter glass bead packs, [18] found trapped gas saturations of similar magnitude to ours (~ 5%), and reported the expected decreasing trend with Ca number, however only for $Ca > 10^{-6}$.

Relationship between initial and residual amounts of non-wetting phase

In Figure 5 we compare *residual* trapped non-wetting area to the *initial* trapped areas. This area vs. area plot is a proxy for the plots presented by [13, 14, 17] which show compiled historic data for residual saturation (S_r) vs initial saturation (S_i) for different types of porous media (consolidated vs. unconsolidated) and fluid pairs. Figure 1 in [13] shows a clear trend of increasing S_r with increasing S_i, but also shows significant variation in this relationship for the different experiments with S_r ranging from 10-65% ([34, 35]'s data). It should be noted that gas is the non-wetting phase in most of the experiments reported by [14]. Additionally, [36] reports that the initial-residual saturation curve varies quite significantly with porous medium type (consolidated vs. unconsolidated, sandstone vs., carbonates, etc.). For data presented here (based on repeated experiments on the same single glass bead core), we have the potential to shed light on trends resulting from use of different fluids (Figure 5). Some of our data (Soltrol and surfactant solutions) also show increasing *residual* trapped NW phase area with increasing *initial* NW phase area, whereas the other fluid pairs are somewhat inconclusive. For the Soltrol experiments with the highest viscosity (and lowest IFT) we see the most significant increase in residual trapping with initial non-wetting phase occupancy. For the other fluid pairs, additional experimentation is needed to provide enough data to establish trends.

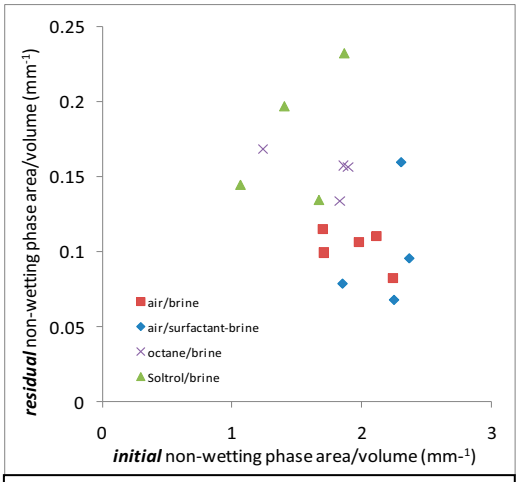

Figure 5. Residual non-wetting phase area as a function of initial non-wetting phase area for the various fluid pairs.

4. Discussion and Conclusion

We report here on experiments carried out to assess the relative importance of fluid interfacial tension, viscosity, and flow rate on the effectiveness of capillary trapping of non-wetting phase for a sintered glass bead pack. To represent the different IFTs and viscosities obtained for CO_2 at different pressures, temperatures, and salinities reported by [2, 20, 21], we used several different fluid pairs and surfactant concentrations. Similar to the many historical data sets summarized by [13, 14, 17], we observed that higher initial amount of trapped non-wetting phase lead to higher residual trapped non-wetting phase (CO_2) for the Soltrol and surfactant solution data. It may therefore be worthwhile to develop injection strategies such that initial non-wetting phase (CO_2) saturation is optimized. Based on these results, increased trapping could be accomplished by injecting CO_2 at a state (P,T relationship-wise) where the lowest viscosity is achieved (see Figure 3) and/or at the lowest injection flow rate (see Figure 4).

The experiments with different imbibition flow rates suggest that once optimal initial non-wetting phase (CO_2) saturation is obtained, the highest amount of trapped non-wetting phase is accomplished by controlling the subsequent imbibition, for instance by an engineered wetting-phase flood, such that the highest possible difference in viscosity between CO_2 and the imbibing fluid is achieved (i.e., the lowest viscosity ratio), and that the flood is carried out at a high flow rate (see Figure 3 and 4). Based on these specific results and on previous work by [19, 32, 37], we believe that CO_2 injection rates can be optimized to facilitate the largest possible amount of trapped residual gas. However, further experimentation on a variety of porous media and for CO_2 under relevant conditions is needed. Also, a larger number of data points are needed to support conclusions based on statistically significant trends, yet we also note that experimentation with x-ray tomography is time-consuming, and requires significant experimental effort. We also wish to reiterate that these results are presented in terms of non-wetting phase area per volume and not saturation, however the trends observed based on areas correlate closely with saturation, and the area data directly support efforts to trap optimal amounts of CO_2 for dissolution trapping. We recommend further experimentation to verify that these trends also hold for consolidated cores, for instance with different aspect ratios that would more favourably support snap-off, and other system properties, however, these types of systems also present additional challenges in terms of imaging and quantification, as does the transition to an experimental setup suitable for supercritical CO_2 conditions.

5. Acknowledgments

Thanks to Matt Tighe and Richard Flavel at University of New England for invaluable support with the UNE x-ray CT system. Thanks also to Trine Wildenschild for measurement of interfacial tensions, and to Tim Kneafsey of LBNL for use of his duNouy tensiometer. This work was supported by project 20100025DR of the Los Alamos Natl. Lab. LDRD program.

6. References

1. Schrag, D.P., *Preparing to capture carbon.* Science, 2007. 315(5813): p. 812-813.
2. IPCC, *IPCC Special Report on Carbon Dioxide Capture and Storage (Intergovernmental Panel on Climate Change, 2005).* available at http://www.ipcc.ch/ipccreports/special-reports.htm. , 2005.
3. Schnaar, G. and D.D. Digiulio, *Computational Modeling of the Geologic Sequestration of Carbon Dioxide.* Vadose Zone Journal, 2009. 8: p. 389-403.
4. Ennis-King, J. and L. Paterson, *Role of convective mixing in the long-term storage of carbon dioxide in deep saline formations.* Spe Journal, 2005. 10(3): p. 349-356.
5. Pruess, K. and J. Garcia, *Multiphase flow dynamics during CO2 disposal into saline aquifers.* Environmental Geology, 2002. 42(2-3): p. 282-295.
6. Flett, M., R. Gurton, and I. Taggart, *The function of gas– water relative permeability hysteresis in the sequestration of carbon dioxide in saline formations.* SPE Pap. 88485-MS, Soc. of Pet. Eng., Richardson, TX., 2004.
7. Juanes, R., et al., *Impact of relative permeability hysteresis on geological CO2 storage.* Water Resources Research, 2006. 42(12).
8. Kumar, A., et al., *Reservoir simulation of CO2 storage in deep saline aquifers.* Spe Journal, 2005. 10(3): p. 336-348.
9. Spiteri, E.J., et al., *Relative permeability hysteresis: Trapping and application to geological CO2 sequestration.* SPE 96448, proceedings of the SPE Annual Meeting, Dallas, Texas. October 2005., 2005.
10. Spiteri, E.J., et al., *A new model of trapping and relative permeability hysteresis for all wettability characteristics.* Spe Journal, 2008. 13(3): p. 277-288.
11. Suekane, T., et al., *Geological storage of carbon dioxide by residual gas and solubility trapping.* International Journal of Greenhouse Gas Control, 2008. 2(1): p. 58-64.
12. Bachu, S. and B. Bennion, *Effects of in-situ conditions on relative permeability characteristics of CO2-brine systems.* Environmental Geology, 2008. 54(8): p. 1707-1722.
13. Pentland, C.H., et al., *Measurement of Non-Wetting Phase Trapping in Sand Packs.* 2008 SPE Annual Technical Conference and Exhibition held in Denver, Colorado, USA, 21–24 September 2008, 2008. SPE 115697.
14. Pentland, C.H., et al., *Measurement of Nonwetting-Phase Trapping in Sandpacks.* Spe Journal, 2010. 15(2): p. 274-281.
15. Land, C.S., *Calculation of imbibition relative permeability for two and three-phase flow from rock properties.* Soc. Pet. Eng. J., 1968. 8(2): p. 149-156.
16. Aissaoui, A., *Etude théorique et expérimentale de l'hystérésis des pressions capillaries et des perméabilitiés relatives en vue du stockage souterrain de gaz.* PhD thesis, Ecole des Mines de Paris, 1983.
17. Al Mansoori, S.K., et al., *Measurements of non-wetting phase trapping applied to carbon dioxide storage.* International Journal of Greenhouse Gas Control, 2009. 4(2): p. 283-288.
18. Suekane, T., et al., *Direct Observation of Trapped Gas Bubbles by Capillarity in Sandy Porous Media.* Transport in Porous Media, 2010. 82: p. 111-122.
19. Perrin, J.-C., et al., *Core-scale experimental study of relative permeability properties of CO2 and brine in reservoir rocks.* Energy Procedia, 2009. 1(3515-3522).
20. Bennion, D.B. and S. Bachu, *A Correlation of the Interfacial Tension between Supercritical-Phase CO2 and Equilibrium Brines as a Function of Salinity, Temperature and Pressure.* Proceedings of the SPE Annual Technical Conference and Exhibition, Denver, CO, Sept 21-24, 2008; SPE Paper 114479., 2008a.
21. Chalbaud, C., et al., *Interfacial tension measurements and wettability evaluation for geological CO2 storage.* Advances in Water Resources, 2009. 32: p. 98-109.
22. Porter, M.L., et al., *Measurement and prediction of the relationship between capillary pressure, saturation, and interfacial area in a NAPL-water-glass bead system.* Water Resources Research, 2010. VOL. 46, W08512, doi:10.1029/2009WR007786.
23. Porter, M.L. and D. Wildenschild, *Validation of an image analysis method for computed microtomography image data of multiphase flow in porous systems.* Journal of Computational Geosciences, 2009. doi: 10.1007/s10596-009-9130-5.
24. Culligan, K.A., et al., *Pore-scale characteristics of multiphase flow in porous media: A comparison of air-water and oil-water experiments.* Advances in Water Resources, 2006. 29(2): p. 227-238.
25. Cense, A.W. and S. Berg, *THE VISCOUS-CAPILLARY PARADOX IN 2-PHASE FLOW IN POROUS MEDIA. International Symposium of the Society of Core Analysts held in Noordwijk, The Netherlands 27-30 September*, 2009.
26. Lake, L.W., *Enhanced Oil Recovery.* Prentice Hall, New Jersey, 1989.
27. Chatzis, I. and N.R. Morrow, *CORRELATION OF CAPILLARY NUMBER RELATIONSHIPS FOR SANDSTONE.* Society of Petroleum Engineers Journal, 1984. 24(5): p. 555-562.
28. Ding, M. and A. Kantzas, *Capillary number correlations for gas-liquid systems.* J. of Canadian Petroleum Technology, 2007. 46(2): p. 27-32.
29. Kantzas, A., M.H. Ding, and J. Lee, *Residual gas saturation revisited.* Spe Reservoir Evaluation & Engineering, 2001. 4(6): p. 467-476.
30. Morrow, N.R., I. Chatzis, and J.J. Taber, *Entrapment and Mobilization of Residual Oil in Bead Packs.* SPE Reservoir Engineering, 1988. 3(3): p. 927-934.
31. Nguyen, V.H., et al. *The effect of displacement rate on imbibition relative permeability and residual saturation*. 2006.
32. Wildenschild, D., et al., *Quantitative analysis of flow processes in a sand using synchrotron-based X-ray microtomography.* Vadose Zone Journal, 2005. 4(1): p. 112-126.
33. Chatzis, I. and N.R. Morrow, *Correlation of capillary number relationships for sandstone.* SPE Journal, 1984. SPE 10114: p. 555-562.
34. Plug, W.J., *Measurements of capillary pressure and electric permittivity of gas-water systems in porous media at elevated pressures.* PhD Thesis, Delft University, 2007.
35. McKay, B.A., *Laboratory studies of gas displacement from sandstone reservoirs having strong water drive. APEA Journal*, 1974: p. 189-194.
36. Stegemeier, G.L., *Mechanisms of Entrapment and mobilization of Oil in Porous Media.* In: Improved Oil Recovery by Surfactant and Polymer Flooding by Shah, D.O. and Schechter, R.S. Ed.; Academic Press, New York., 1977.
37. Wildenschild, D., J.W. Hopmans, and J. Simunek, *Flow rate dependence of soil hydraulic characteristics.* Soil Science Society of America Journal, 2001. 65(1): p. 35-48.